Vortex Generation Through Balanced Adjustment

JAMES C. MCWILLIAMS

National Center for Atmospheric Research, Boulder, Colorado*

(Manuscript received 23 September 1987, in final form 23 February 1988)

ABSTRACT

The problem of geostrophic adjustment, originally considered by C. G. Rossby, is solved in an axisymmetric geometry for a continuously stratified fluid, where the adjusted final state is in hydrostatic, gradient-wind balance. This problem is relevant to the generation of submesoscale coherent vortices in the ocean: diapycnal mixing events can create a local anomaly of less strongly stratified fluid, which then develops a balancing circulation through adjustment. An analytic solution is obtained for a few uniform-density layers, and this is compared with numerical solutions for continuous stratification. In both representations, two-dimensional solutions are compared with axisymmetric ones.

1. Introduction

Submesoscale Coherent Vortices (SCVs) are abundant in the interior of the ocean (McWilliams 1985). These are intense, rotary circulations which are approximately symmetric about vertical axes. Typical dimensions are 10 km horizontally and 100 m vertically. SCV lifetimes can be as long as many years, during which entire ocean basins can be traversed.

In McWilliams (1985) I argued that the principal generation mechanism for SCVs is mixing and adjustment: local mixing in a stratified environment creates a region of weaker stratification, and the subsequent adjustment process creates a balancing circulation. SCVs are observed to be always of one parity, anticyclonic, and this generation mechanism intrinsically has this parity.

Adjustment has to date been investigated for geostrophic balance, usually for parallel flow, and often with a linearization assumption (Rossby 1937, 1938; Obukhov 1949; see Blumen 1972 for a review). The circumstances of SCVs require centrifugal force as well as Coriolis and pressure forces in the momentum balance (i.e., gradient wind balance), the flow geometry is cylindrical rather than parallel, and several relations are significantly nonlinear.

As a contribution towards assessing the plausibility of SCV generation by mixing and adjustment, the following idealized problem is posed and solved below. In an unbounded, incompressible, uniformly stratified fluid, mixing across isopycnals is presumed to have created an initial state with a local density anomaly (heavy above, light below, with an amplitude bounded by marginal static stability) and no motion. The anomaly shape is assumed to be independent of the azimuthal coordinate and odd-symmetric about its middle depth. Gravitational force then acts to compress the anomaly in the vertical near its center and, by incompressibility, to extrude fluid horizontally outward. The subsequent evolution involves radiation of inertial–gravity waves away from the anomaly and the development of a balancing circulation as the Coriolis force turns the radial motion towards the azimuthal direction. At a time much greater than the longest wave period (of order inverse Coriolis frequency), the waves will have departed, and the local circulation will be steady and in hydrostatic, gradient-wind balance. If viscous and diabatic processes are neglected, the adjusted state will have, for every fluid parcel, the same density, angular momentum, and potential vorticity as initially, with, of course, the fluid parcels displaced so as to satisfy the balance relations. The energy of the final state, however, will be reduced from the initial state energy, with the deficit lost through wave radiation to infinity. We seek to determine the final state (the SCV) as a function of the initial one (the density anomaly from mixing). Of course, the solutions obtained may have more general applicability than just to the SCV phenomenon.

2. Adjustment of a layered fluid

As a prelude to solving the fully continuous problem, we consider adjustment in the sparser representation of a few layers with different but internally uniform densities. This will illustrate many of the qualitative

* The National Center for Atmospheric Research is supported by the National Science Foundation.

Corresponding author address: Dr. James C. McWilliams, NCAR, P.O. Box 3000, Boulder, CO 80307.

features of adjustment in general, through an explicit, closed form solution.

Consider the layer geometry in Fig. 1. There are five layers (by vertical symmetry only three are independent). The core layer has a density ρ_* and a finite volume: its half thickness $h(r)$ goes to zero at a finite radius r_0. The outer layers have densities $\rho_*(1 \pm \delta)$ and thickness $H(r)$, which has the value H_∞ as $r \to \infty$. Finally, the exterior layers have densities $\rho_*(1 \pm \delta \pm \Delta)$, infinite thickness, and neither any motion nor any horizontal pressure gradient.

In this representation, the mixing is presumed to have created the core layer. Initially, the azimuthal velocity $v(r)$ is zero. The volume of fluid (per unit radian) in the core layer inside radius r is

$$V(r) = \int_0^r r'h(r')dr', \tag{1}$$

with an analogous expression for the outer layer (i.e., with $h \to H$). (Because of the assumed symmetry, only the half space $z \geq 0$ is included here.) The potential vorticity and angular momentum are

$$q = \frac{f}{h} \quad \text{or} \quad \frac{f}{H}, \quad \text{and}$$

$$A = \tfrac{1}{2}fr^2, \tag{2}$$

where f is the Coriolis frequency. Finally the initial potential energy (per unit radian) is

$$\text{PE} = \tfrac{1}{2}g\int_0^\infty [\delta h^2 + \Delta(H+h)^2 - \Delta H_\infty^2]rdr, \tag{3}$$

and, of course, the kinetic energy is zero.

In the final state, the pressure is hydrostatic; thus,

$$p = \begin{cases} \rho_* g\Delta(H+h), & \text{outer} \\ \rho_* g\Delta(H+h) + \rho_* g\delta h, & \text{core,} \end{cases} \tag{4}$$

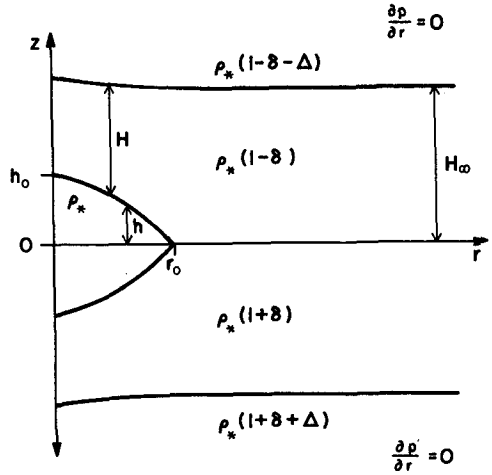

FIG. 1. Geometry of a layered fluid.

plus terms that are independent of r. The associated circulation is in gradient wind balance:

$$fv + \frac{v^2}{r} = \frac{1}{\rho_*}\frac{dp}{dr}$$

or

$$v = \frac{fr}{2}\{S-1\}, \quad S = \left\{1 + \frac{4}{(\rho_* f^2 r)}\frac{dp}{dr}\right\}^{1/2}. \tag{5}$$

Relative, absolute, and potential vorticities and angular momentum are defined by

$$\zeta = \frac{1}{r}\frac{\partial}{\partial r}(rv), \quad Z = f + \zeta,$$

$$q = \frac{Z}{h} \quad \text{or} \quad \frac{Z}{H},$$

$$A = \tfrac{1}{2}fr^2 + vr = \tfrac{1}{2}fr^2 S. \tag{7}$$

Volume and PE are defined as in (3) and (1), and kinetic energy (per unit radian) is

$$\text{KE} = \tfrac{1}{2}\int_0^\infty [hv_{\text{core}}^2 + Hv_{\text{outer}}^2]rdr. \tag{8}$$

The adjustment problem can now be posed in terms of Lagrangian time integrals of the parcel conservation relations. Let ξ be the radial displacement of a parcel in the core layer, such that

$$r_{\text{initial}} = r_{\text{final}} - \xi(r_{\text{final}}), \tag{9}$$

and let Ξ be the analogous displacement in the outer layer. Then the conservation of mass, angular momentum, and potential vorticity in the core layer is expressed by

$$V_s(r) = V_m(r - \xi(r))$$

$$A_s(r) = A_m(r - \xi(r))$$

$$q_s(r) = q_m(r - \xi(r)), \tag{10}$$

where subscripts m and s refer to the initial mixing anomaly and the final SCV, respectively; analogous relations hold in the outer layer.

Given $h(r)$ and $H(r)$ initially, we seek the four final state functions ξ, Ξ, h and H which are solutions of the six parcel conservation relations in the core and outer layers. By this counting the problem appears to be overdetermined, which it is not. From (1), (6) and (7), we write

$$q = \frac{(1/2r)d/dr(r^2S)}{h} = \frac{(1/r)dA/dr}{(1/r)dV/dr} = \frac{dA/dr}{dV/dr}.$$

From the first two relations in (10),

$$\frac{dA_s}{dr}(r) = \frac{dA_m}{dr}(r-\xi)\cdot\left[1-\frac{d\xi}{dr}\right],$$

$$\frac{dV_s}{dr}(r) = \frac{dV_m}{dr}(r-\xi)\cdot\left[1-\frac{d\xi}{dr}\right];$$

hence,

$$q_s(r) = \frac{dA_s/dr(r)}{dV_s/dr(r)} = \frac{dA_m/dr(r-\xi)}{dV_m/dr(r-\xi)} = q_m(r-\xi).$$

Thus, one conservation relation among the three above is redundant in each layer, and the problem is well determined.

The preceding relations are valid for arbitrary anomaly profiles $h_m(r)$ and $H_m(r)$. An approximate, closed form solution can be found for the mixing anomaly

$$h_m(r) = \begin{cases} h_{0m}\left[1-\left(\dfrac{r}{r_{0m}}\right)^2\right], & r \leqslant r_{0m} \\ 0, & r > r_{0m} \end{cases} \qquad (11)$$

$$H_m(r) = -h_m(r) + H_\infty.$$

(The second relation states that the initial anomaly is of limited vertical extent.) This quadratic profile leads to radially uniform relative and absolute vorticity in the core layer [see (12) below]. In somewhat different layered configurations, axisymmetric solutions with uniform potential vorticity are presented in Csanady (1979), Flierl (1979), and Ikeda (1982).

When the outer layer is deep (i.e., $\epsilon = h_{0m}/H_\infty \ll 1$), its pressure variations (4) are negligible in the core layer relations (10). Thus, to $O(\epsilon)$ the core layer solution is

$$h_s(r) = h_{0s}\left[1-\left(\frac{r}{r_{0s}}\right)^2\right],$$

$$\xi_s(r) = \xi_{0s}\frac{r}{r_{0s}}$$

$$v_s(r) = v_{0s}\frac{r}{r_{0s}}$$

$$\zeta_s(r) = 2\frac{v_{0s}}{h_{0m}}$$

$$Z_s(r) = f\frac{h_{0s}}{h_{0m}} \qquad (12)$$

for $r \leqslant r_{0s}$, outside of which the core layer does not exist. The constants in (12) are

$$\frac{h_{0s}}{h_{0m}} = \frac{Z_s}{f} = T^{-1/2} \quad \epsilon(0,1)$$

$$\frac{r_{0s}}{r_{0m}} = T^{1/4} \quad \epsilon(1,\infty)$$

$$\frac{\xi_{0s}}{r_{0s}} = 1 - T^{-1/4} \quad \epsilon(0,1)$$

$$\frac{v_{0s}}{fr_{0s}} = -\frac{1}{2}(1-T^{-1/2}) \quad \epsilon\left(-\frac{1}{2},0\right) \qquad (13)$$

for

$$T = 1 + 8b \quad \text{and} \quad b = \frac{g\delta h_{0m}}{f^2 r_{0m}^2} > 0. \qquad (14)$$

Thus, the core layer undergoes a gravitational flattening and spreading, and it has anticyclonic flow with a constant vorticity bounded from below by $-f$. Note that the volume scale $h_0 r_0^2$ is preserved during adjustment.

The outer layer volume conservation relation can be written

$$\Xi(r) = \frac{1}{H_\infty r}\int_0^r [h_s(r') - h_m(r')]r'dr' + O(\epsilon). \qquad (15)$$

The solution in the outer layer is

$$H_s(r) = H_\infty - h_s(r), \quad r \leqslant r_{0s}$$
$$= H_\infty, \quad r > r_{0s}$$

$$\Xi(r) = \frac{1}{2}\epsilon r\left[-(1-T^{-1/2}) + \frac{1}{2}(1-T^{-1})\left(\frac{r}{r_{0m}}\right)^2\right],$$
$$r \leqslant r_{0m}$$
$$= \frac{1}{2}\epsilon r T^{-1/2}\left[1 - \frac{1}{2}\left(\frac{r}{r_{0s}}\right)^2 - \frac{1}{2}\left(\frac{r_{0s}}{r}\right)^2\right],$$
$$r_{0m} < r \leqslant r_{0s}$$
$$= 0, \quad r > r_{0s}$$

$$v_s(r) = \frac{1}{2}\epsilon fr\left[1 - T^{-1/2} - \frac{1}{2}(1-T^{-1})\left(\frac{r}{r_{0m}}\right)^2\right],$$
$$r \leqslant r_{0m}$$
$$= \frac{1}{2}\epsilon fr T^{-1/2}\left[-1 + \frac{1}{2}\left(\frac{r}{r_{0s}}\right)^2 + \frac{1}{2}\left(\frac{r_{0s}}{r}\right)^2\right],$$
$$r_{0m} < r \leqslant r_{0s}$$
$$= 0, \quad r > r_{0s}$$

$$\zeta_s(r) = \epsilon f\left[1 - T^{-1/2} - (1-T^{-1})\left(\frac{r}{r_{0m}}\right)^2\right],$$
$$r \leqslant r_{0m}$$
$$= -\epsilon f T^{-1/2}\left[1 - \left(\frac{r}{r_{0s}}\right)^2\right], \quad r_{0m} < r \leqslant r_{0s}$$
$$= 0, \quad r > r_{0s} \qquad (16)$$

with relative errors $O(\epsilon)$. We see that all outer layer quantities have an amplitude factor ϵ, demonstrating a posteriori the consistency of the core layer decoupling

approximation described above. The Ξ is negative $\forall\, r < r_{0s}$; thus, the horizontal spreading of the core layer is compensated by a contraction in the outer layer. Therefore, by angular momentum conservation, the outer layer circulation has $v_s > 0\ \forall\, r < r_{0s}$. However, its vorticity changes sign at

$$r = r_{0m}\cdot\left[\frac{T - T^{1/2}}{T-1}\right]^{1/2} \quad \epsilon\left(\frac{r_{0m}}{2}, r_{0m}\right). \tag{17}$$

Within this radius ζ_s is cyclonic, which is the reverse of the anticyclonic core layer vorticity.

The circulation in the outer layer,

$$C_s = \int_0^\infty \zeta_s(r) r dr, \tag{18}$$

is zero from (15). (Circulation is not well defined for the core layer, since it does not extend to infinity.) Azimuthal transport, however, is finite:

$$\begin{aligned}
\mathrm{Tr}(r) &\equiv h_s v_{s,\mathrm{core}}(r) + H_s v_{s,\mathrm{outer}}(r),\\
&= \tfrac{1}{2} f h_{0m} r (1 - T^{-1/2})\Big[1 - T^{-1/2} - \Big(\tfrac{1}{2} T^{1/2}\\
&\qquad + \tfrac{1}{2} - T^{-1/2}\Big)\Big(\frac{r}{r_{0s}}\Big)^2\Big], \quad r \leqslant r_{0m}\\
&= \tfrac{1}{2} f h_{0m} r T^{-1/2}\Big[-2 + T^{-1/2} + \Big(\tfrac{3}{2} - T^{-1/2}\Big)\\
&\qquad \times \Big(\frac{r}{r_{0s}}\Big)^2 + \frac{1}{2}\Big(\frac{r_{0s}}{r}\Big)^2\Big], \quad r_{0m} < r \leqslant r_{0s}\\
&= 0, \quad r > r_{0s}.
\end{aligned} \tag{19}$$

This is positive (opposite the core layer transport) inside the radius

$$r = r_{0m}\left(\frac{2}{1 + T^{1/2}}\right)^{1/2} \quad \epsilon(0, r_{0m}) \tag{20}$$

and negative between there and r_{0s}. Integrated in r,

$$\begin{aligned}
\int_0^\infty \mathrm{Tr}(r) r dr &= \int_0^\infty \int_0^\infty v r dr dz\\
&= \tfrac{1}{15} f h_{0m} r_{0m}^3 [T^{1/4} + T^{-1/4} - 1],
\end{aligned} \tag{21}$$

which is always positive (i.e., cyclonic).

Inserting the solutions (12) and (15) into (3) and (8) yields

$$\begin{aligned}
\frac{(\mathrm{KE}_s + \mathrm{PE}_s)}{\mathrm{PE}_m} &= \frac{4}{3} T^{-1/2} \frac{(1 + \frac{1}{2} T^{-1/2})}{(1 + T^{-1/2})},\\
\frac{\mathrm{KE}_s}{\mathrm{PE}_s} &= \frac{(1 - T^{-1/2})}{(1 + T^{-1/2})},
\end{aligned} \tag{22}$$

where the contributions from the outer layer fields are negligible [i.e., $O(\epsilon)$]. Both of these ratios are always between zero and one; thus, adjustment inevitably requires a loss of energy, and the SCV kinetic energy cannot exceed its potential energy.

This solution is characterized by its size, amplitude, and shape. In (12)–(22), the dependence of the first two attributes is relatively simple, in large measure because, in this simple layer formulation, the environment does not have any natural size or amplitude measures. Variations of shape (here the aspect ratio h_0/r_0) are more complex but they depend only on the parameter b from (14). b has the form of a Burger number (or inverse Froude number), except that the deformation radius, $(g\delta h_{0m})^{1/2} f^{-1}$, is based upon the disturbance amplitude (since the environment lacks a relevant scale). This intrinsic combination of disturbance amplitude and shape is a consequence of the sparse layer representation. It also precludes a quasi-geostrophic solution to the present problem. These aspects will be separated in the continuously stratified problem solved below.

As b increases from small to large values (due to a larger density difference or core layer thickness, or a smaller core layer width), the adjustment process yields larger shape change, stronger vorticity and velocity, larger transport, greater relative energy loss, and greater relative kinetic energy. Thus, a SCV with these attributes results from a mixing anomaly of larger aspect ratio, h_{0m}/r_{0m}, as it enters the Burger number,

$$b = \frac{g\delta}{h_{0m} f^2}\left(\frac{h_{0m}}{r_{0m}}\right)^2 = \frac{N^2}{f^2}\left(\frac{h_{0m}}{r_{0m}}\right)^2, \tag{23}$$

where N is a buoyancy frequency.

3. A two-dimensional layered comparison

The two-dimensional (2D) counterpart of the axisymmetric problem will be solved here for comparison. We assume the same layered geometry as in Fig. 1, where r is now considered a Cartesian horizontal coordinate. The three parcel-conservative quantities in 2D are

$$\begin{aligned}
V(r) &= \int_0^r h(r') dr',\\
q &= \frac{Z}{h} \quad \text{or} \quad \frac{Z}{H},\\
A &= fr + v,
\end{aligned} \tag{24}$$

and the balance relation is exactly geostrophic,

$$v = \frac{1}{f\rho_*}\frac{dp}{dr}. \tag{25}$$

Vorticity in 2D is

$$\zeta = \frac{dv}{dr}. \tag{26}$$

The horizontal integrals PE, KE, C, and $\int \mathrm{Tr}$ all have dr in place of rdr.

In 2D the initial profile (11) has a solution in the core layer of nearly the same form as (12), except for

$$v_s(r) = 2v_{0s}\left(\frac{r}{r_{0s}}\right). \tag{27}$$

However, the constants are different from (13); viz.,

$$\frac{h_{0s}}{h_{0m}} = \frac{Z_s}{f} = U^{-1/3} \quad \epsilon(0, 1)$$

$$\frac{r_{0s}}{r_{0m}} = U^{1/3} \quad \epsilon(1, \infty)$$

$$\frac{\xi_{0s}}{r_{0s}} = 1 - U^{-1/3} \quad \epsilon(0, 1)$$

$$\frac{v_{0s}}{fr_{0s}} = -\frac{1}{2}(1 - U^{-1/3}) \quad \epsilon\left(-\frac{1}{2}, 0\right), \tag{28}$$

where $U(b)$ is the solution of

$$(U - 2b)^3 - U^2 = 0 \tag{29}$$

for b from (14). As b increases from zero to $+\infty$, $U(b)$ increases from one to $+\infty$. Here it is the product of h_0r_0 which is preserved during adjustment.

There is considerable similarity between the 2D and axisymmetric solutions. The constants in (13) and (28) all have monotonic dependences upon b and span the same ranges of values. The detailed functional dependences are different, though. To examine these differences, we consider the relations between $T(b)$ and $U(b)$ from (14) and (29); in particular,

$$\begin{aligned} &U^{-1/3} = T^{-1/4} = T^{-1/2} = 1 \quad \text{at} \quad b = 0 \\ &U^{-1/3} \gtrsim T^{-1/4} > T^{-1/2} \quad \text{for} \quad 0 < b < 32 \\ &T^{-1/4} > U^{-1/3} > T^{-1/2} \quad \text{for} \quad b > 32, \end{aligned} \tag{30}$$

where $U^{-1/3}$ never exceeds $T^{-1/4}$ in the lower range of b by more than about 2%. The near equality of $U^{-1/3}$ and $T^{-1/4}$ implies that the horizontal particle displacements are quite similar between 2D and axisymmetric adjustment. However, $U^{-1/3} > T^{-1/2}$ indicates that the vertical displacements are larger in axisymmetric adjustment, as is the magnitude of the SCV relative vorticity. On the other hand, the azimuthal velocity is larger in 2D, due in part to the extra factor of two in (27), although the difference is not appreciable for $b < 1$. Although the balance relations imply that, for a given pressure gradient, the velocity is larger in an axisymmetric geometry than in 2D, the pressure gradient is sufficiently larger in 2D to overcome this effect.

The outer layer solution in 2D is also qualitatively similar to axisymmetric adjustment, hence so are the circulation and transport integrals. The energy ratios corresponding to (22) are

$$\frac{(\mathrm{KE}_s + \mathrm{PE}_s)}{\mathrm{PE}_m} = \frac{1}{2}U^{-1/3}[3 - U^{-1/3}]$$

$$\frac{\mathrm{KE}_s}{\mathrm{PE}_s} = \frac{1}{2}[1 - U^{-1/3}]. \tag{31}$$

(31) exhibits the same qualitative dependence upon b as (22). At any particular $b > 0$, however, the axisymmetric adjustment process has a relative greater energy loss than 2D, and its proportion of kinetic energy is also larger.

In summary, the adjustment process effects a greater change (in energy, in vorticity) in an axisymmetric geometry than in a two-dimensional one.

4. Adjustment of a continuously stratified fluid

We now consider the complete problem posed in the Introduction. The equations are made nondimensional with the following scaling factors:

$$\begin{aligned} &r \sim l_* && \rho \sim \rho_* N_*^2 \frac{h_*}{g} \\ &z \sim h_* && A \sim l_*^2 \\ &v \sim v_* && q \sim fN_*^2 \\ &p \sim \rho_* v_* f l_* && (\mathrm{KE}, \mathrm{PE}) \sim h_* l_*^2 v_*^2 \\ &\zeta \sim \frac{v_*}{l_*} && \mathrm{Tr} \sim v_* h_*. \end{aligned} \tag{32}$$

Associated parameters are

$$R = \frac{4v_*}{fl_*}$$

$$B = \left(\frac{N_* h_*}{fl_*}\right)^2$$

$$\gamma = \frac{R}{4B}. \tag{33}$$

The mixing-induced density anomaly $\Theta(r, z)$ has a dimensional scale $\rho_* v_* f l_*/g h_*$, such that the nondimensional total density field is

$$\rho_m = -z + \gamma\Theta. \tag{34}$$

Hence

$$N_m \equiv \left\{-\frac{\partial \rho_m}{\partial z}\right\}^{1/2} = \left\{1 - \gamma\frac{\partial \Theta}{\partial z}\right\}^{1/2} \tag{35}$$

is the initial buoyancy frequency. The nondimensional potential vorticity and angular momentum fields are

$$q_m = N_m^2$$

$$A_m = \frac{1}{2}r^2, \tag{36}$$

and the energy of the anomaly is

$$\mathrm{PE}_m = \frac{1}{2B}\int_0^\infty rdr \int_0^\infty dz\, \Theta^2. \tag{37}$$

After adjustment, hydrostatic, gradient-wind balance implies the following relations for the SCV:

$$\rho_s = -z - \gamma \frac{\partial p}{\partial z}$$

$$N_s^2 = 1 + \gamma \frac{\partial^2 p}{\partial z^2}$$

$$v = \frac{2r}{R}[S-1]$$

$$S = \left\{1 + \frac{R}{r}\frac{\partial p}{\partial r}\right\}^{1/2}$$

$$\zeta = \frac{1}{r}\frac{\partial (rv)}{\partial r}$$

$$Z = 1 + \frac{R}{4}\zeta = S + \frac{r}{2}\frac{\partial S}{\partial r}$$

$$q_s = ZN_s^2 - \frac{R\gamma}{4S}\left(\frac{\partial^2 p}{\partial r \partial z}\right)^2$$

$$A_s = \frac{1}{2}r^2 + \frac{R}{4}vr = \frac{1}{2}r^2 S$$

$$\mathrm{KE}_s = \frac{1}{2}\int_0^\infty rdr \int_0^\infty dz v^2$$

$$\mathrm{PE}_s = \frac{1}{2B}\int_0^\infty rdr \int_0^\infty dz \left(\frac{\partial p}{\partial z}\right)^2. \tag{38}$$

q in (36) and (38) is Ertel potential vorticity, the scalar product of the absolute vorticity vector and the density gradient.

As in the layered problem, we are concerned with Lagrangian displacements during adjustment, here defined as

$$\gamma \xi(r_f, z_f) = r_f - r_i$$
$$\gamma \eta(r_f, z_f) = z_f - z_i, \tag{39}$$

where the subscripts denote final and initial parcel positions. Fluid incompressibility requires that the Jacobian of a Lagrangian coordinate transformation be equal to unity (Monin and Yaglom 1971). In an axisymmetric geometry, this is expressed by

$$\frac{r_i}{r_f}\left(\frac{\partial r_i}{\partial r_f}\frac{\partial z_i}{\partial z_f} - \frac{\partial r_i}{\partial z_f}\frac{\partial z_i}{\partial r_f}\right) = 1,$$

or, from (39),

$$\frac{1}{r}\frac{\partial}{\partial r}(r\xi) = \left(1 - \gamma\frac{\xi}{r}\right)\left(-\frac{\partial \eta}{\partial z} + \gamma\frac{\partial \xi}{\partial r} \times \frac{\partial \eta}{\partial z} - \gamma\frac{\partial \xi}{\partial z}\frac{\partial \eta}{\partial r}\right) + \gamma\frac{\xi}{r}\frac{\partial \xi}{\partial r}. \tag{40}$$

The parcel conservation relations for continuously stratified adjustment are

$$\rho_s(r, z) = \rho_m(r - \gamma\xi(r, z), z - \gamma\eta(r, z))$$
$$q_s(r, z) = q_m(r - \gamma\xi(r, z), z - \gamma\eta(r, z))$$
$$A_s(r, z) = A_m(r - \gamma\xi(r, z), z - \gamma\eta(r, z)). \tag{41}$$

(40) and (41) comprise four relations for the three unknowns p, ξ and η. Again there is a redundancy by one relation, and we will discard angular momentum conservation in our method of solution. Boundary conditions are

$$(p, \xi, \eta) \to 0 \quad \text{as} \quad r^2 + z^2 \to \infty$$
$$\xi = \frac{\partial p}{\partial r} = 0 \quad \text{at} \quad r = 0$$
$$\eta = \frac{\partial p}{\partial z} = 0 \quad \text{at} \quad z = 0. \tag{42}$$

Because the equations are nonlinear an iterative method is used; viz.,

$$\rho^{(0)} = \xi^{(0)} = \eta^{(0)} = 0,$$

$$n = 1, 2, \cdots \begin{cases} \dfrac{B}{r}\dfrac{\partial}{\partial r}\left(r\dfrac{\partial p^{(n)}}{\partial r}\right) + \dfrac{\partial^2}{\partial z^2}p^{(n)} = -\dfrac{\partial \Theta}{\partial z} \times (r - \gamma\xi^{(n-1)}, z - \gamma\eta^{(n-1)}) - \gamma \cdot \delta q_s[p^{(n-1)}] \\ \eta^{(n)} = -\Theta(r - \gamma\xi^{(n-1)}, z - \gamma\eta^{(n-1)}) - \dfrac{\partial p^{(n)}}{\partial z} \\ \xi^{(n)} = \dfrac{1}{r}\displaystyle\int_0^r r'dr' C[\eta^{(n)}, \xi^{(n-1)}]. \end{cases} \tag{43}$$

These relations are, respectively, the conservation of q and ρ from (38) and (41) and the incompressibility condition (40) (with $C[\eta, \xi]$ its right-hand side). The nonquasi-geostrophic component of potential vorticity δq_s is defined by

$$\delta q_s[p] \equiv \gamma^{-1}(q_s - 1) - \frac{B}{r}\frac{\partial}{\partial r}\left(r\frac{\partial p}{\partial r}\right) - \frac{\partial^2 p}{\partial z^2}$$
$$= B\frac{1-S}{S}\frac{\partial^2 p}{\partial r^2} - B\frac{(1-S)^2}{S(1+S)}\frac{1}{r}\frac{\partial p}{\partial r} + (S-1)\frac{\partial^2 p}{\partial z^2} + \frac{R}{4S}\left(\frac{\partial^2 p}{\partial r^2} - \frac{1}{r}\frac{\partial p}{\partial r}\right)\frac{\partial^2 p}{\partial z^2} - \frac{R}{4S}\left(\frac{\partial^2 p}{\partial r \partial z}\right)^2. \tag{44}$$

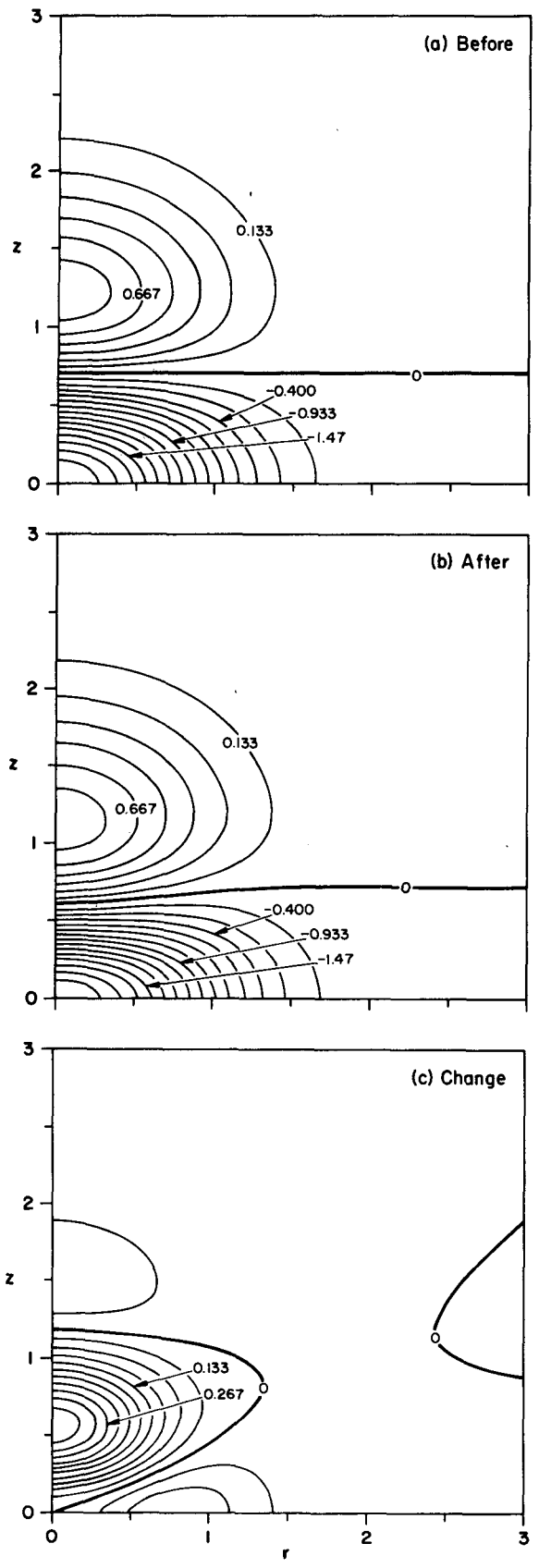

We adopt the following normalization conventions and functional form for the initial anomaly. Let Θ have the form

$$\Theta = 2ze^{-\mu^\beta} \tag{45}$$

for

$$\mu = z^2 + \left(\frac{r}{r_{0m}}\right)^2 \tag{46}$$

and β a positive constant. This satisfies the conditions

$$\begin{aligned} &\int_{-\infty}^{\infty} dz\Theta = 0, \\ &\Theta \to 0 \quad \text{as} \quad \mu \to \infty, \\ &\Theta = 0 \quad \text{at} \quad z = 0 \\ &\frac{\partial \Theta}{\partial r} = 0 \quad \text{at} \quad r = 0, \end{aligned} \tag{47}$$

consistent with mixing having acted only locally and with the symmetries stated in the Introduction. Furthermore,

$$\frac{\partial \Theta}{\partial z}(0, 0) = 2,$$

so that $\gamma \epsilon (0, 1/2)$ spans the range of statically stable initial states in (35). Finally, given the radial scale r_{0m} in (46), we set $B = 1$ without loss of generality, hence $R = 4\gamma$. Therefore, the initial anomaly is fully prescribed by an amplitude γ, a radial scale r_{0m}, and a profile steepness parameter β. More fundamentally, perhaps, r_{0m}^{-1} is a normalized aspect ratio for the mixing anomaly, based upon its radial and vertical dimensions and the environmental quantities N_* and f.

We are also interested in a posteriori measures of the SCV solution to (40)–(46). Consider a rescaling of the solution by nondimensional pressure and coordinate scales p_{0s}, r_{0s} and z_{0s} such that, after rescaling,

$$\begin{aligned} p(0, 0) &= 1 \\ Z(0, 0) &= \sqrt{1 - 2R_s} \\ N_s^2(0, 0) &= 1 - \frac{R_s}{2B_s}, \end{aligned} \tag{48}$$

where

$$\begin{aligned} R_s &= R\frac{p_{0s}}{r_{0s}^2} \\ B_s &= B\frac{z_{0s}^2}{r_{0s}^2} \end{aligned} \tag{49}$$

FIG. 2. Potential vorticity anomaly $\gamma^{-1}(q(r, z) - 1)$ for $\gamma = 0.25$, $r_{0m} = 1$, $\beta = 1$: (a) before adjustment, contour interval (c.i.) = 0.133; (b) after adjustment, c.i. = 0.133; (c) difference due to adjustment, c.i. = 0.033.

are SCV Rossby and Burger numbers. The relations (48) are obtained from a kinematic SCV model in McWilliams (1985). Note the bounds

$$R_s \leqslant \frac{1}{2}, \quad R_s \leqslant 2B_s \tag{50}$$

for the existence of a SCV of the general shape being considered here.

An approximate solution to the adjustment problem may be obtained by taking the limit $(R, \gamma) \to 0$ in (40)–(46); this is the quasigeostrophic (QG) limit. This has the advantage of simplicity, since the governing relations become full linear in the fields p, ξ, and η, hence (43) can be solved completely at $n = 1$.

Now consider a particular SCV solution for a mixing anomaly of intermediate strength ($\gamma = 0.25$), unit normalized aspect ratio ($r_{0m} = 1$), and Gaussian shape ($\beta = 1$).

The q anomaly initially has a minimum at the center of the mixing region, with a lesser maximum above it (Fig. 2a). After adjustment, q has a similar pattern (Fig. 2b), with the largest changes occurring away from the q extrema (Fig. 2c).

The SCV pressure field has a high value at the core, with a low above (Fig. 3a). This corresponds to an anticyclonic circulation about the central high with much weaker cyclonic velocities about the low (Fig. 3b). The vorticity, though, shows a four center pattern (Fig. 3c), and the circulation

$$C(z) = \int_0^\infty r dr \zeta(r, z) \tag{51}$$

is equal to zero at all z, to within small numerical errors. The azimuthal transport

$$T_r(r) = \int_0^\infty dz v(r, z) \tag{52}$$

is zero at $r = 0$, has a maximum of 0.012 at $r = 0.49$, is zero at $r = 1.20$, has a minimum of -0.002 at $r = 1.65$, and decays to zero as $r \to \infty$. All of these features have a qualitative correspondence with those of the layered solution in section 2.

The SCV density anomaly has a positive extremum above the core (Fig. 3d), as in the mixing anomaly (45), but it also has a weak minimum further above that, due to sinking motions along the axis (Fig. 3g). The SCV stratification anomaly (Fig. 3e) also shows an additional extremum at ($r = 0$, z large); for comparison, the field in Fig. 2a is the identical quantity $\gamma^{-1}(N_m^2 - 1)$ before adjustment. The Lagrangian displacements (Fig. 3f, g) have much larger amplitude in the core region of gravitational collapse (downward and outward); the displacements are smaller in the peripheral zone of upward and inward motion.

The a posteriori SCV measures (48)–(49) have the following values:

$$R_s = 0.181$$

$$B_s = 0.241$$

$$r_{0s} = 1.350$$

$$z_{0s} = 0.663$$

$$p_{0s} = 0.329.$$

Thus, during adjustment, the height has diminished from $z_{0m} = 1$, the horizontal extent has increased from $r_{0m} = 1$, the aspect ratio has changed from 1.00 to 0.49, and the intensity measure R_s is 36% of its upper bound (50) while the initial intensity γ is 50% of its bound. The energy ratios are

$$\frac{(\mathrm{KE}_s + \mathrm{PE}_s)}{\mathrm{PE}_m} = 0.605$$

$$\frac{\mathrm{KE}_s}{\mathrm{PE}_s} = 0.389.$$

Each of these values can be found within the ranges spanned by the layered solution as a function of b. However, it is not possible to simultaneously come close to all of them for any particular b value.

We now examine the amplitude dependence of adjustment, which is not possible in the layered approximation. The variation of SCV parameters with $\gamma \in (0, 0.5)$ is listed in Table 1. ($\gamma = 0.49$ is included instead of $\gamma = 0.50$, since the rate of convergence of the iteration sequence (43) goes to zero as $\gamma \to 0.5$.) The most obvious dependence is that the amplitude of the SCV (e.g., R_s) increases with γ. The other parameters in Table 1 show somewhat less strong dependences, and none of the dependences depart too strongly from a linear function of γ. Relative to QG, a balanced SCV has a smaller aspect ratio (i.e., greater gravitational slump), a larger velocity and azimuthal transport[1] (n., these nondimensional quantities in (32) have been scaled by factors proportional to γ), a diminished energy loss during adjustment, and a smaller kinetic energy fraction.

In Fig. 4 the ratio R_s/γ is plotted; this is a measure of the efficiency of SCV generation by adjustment. Here it has values less than one [assuring the first bound in (50)] and is a decreasing function of γ. Also plotted is $R_s/2B_s$, which appears in the second bound in (50). This is an increasing function of γ, which is to be expected since $dR_s/d\gamma > 0$. Note that it, in fact, does approach its limiting value of one as γ approaches 0.5; thus the strongest SCV (for fixed r_{0m} and β) has the smallest possible aspect ratio, consistent with static stability in the core. This limit for $R_s/2B_s$ has been confirmed for many different r_{0m} and β values. Therefore, we summarize the asymptotic limits in γ by

$$R_s \to 0 \quad \text{as} \quad \gamma \to 0$$

$$\frac{R_s}{2B_s} \to 1 \quad \text{as} \quad \gamma \to \frac{1}{2}. \tag{53}$$

[1] In the QG limit, $\mathrm{Tr}(r) = 0$ since $v \propto \xi$ from conservation of A in (41) and $\int_0^\infty \xi dz = 0$ from (40) and (42).

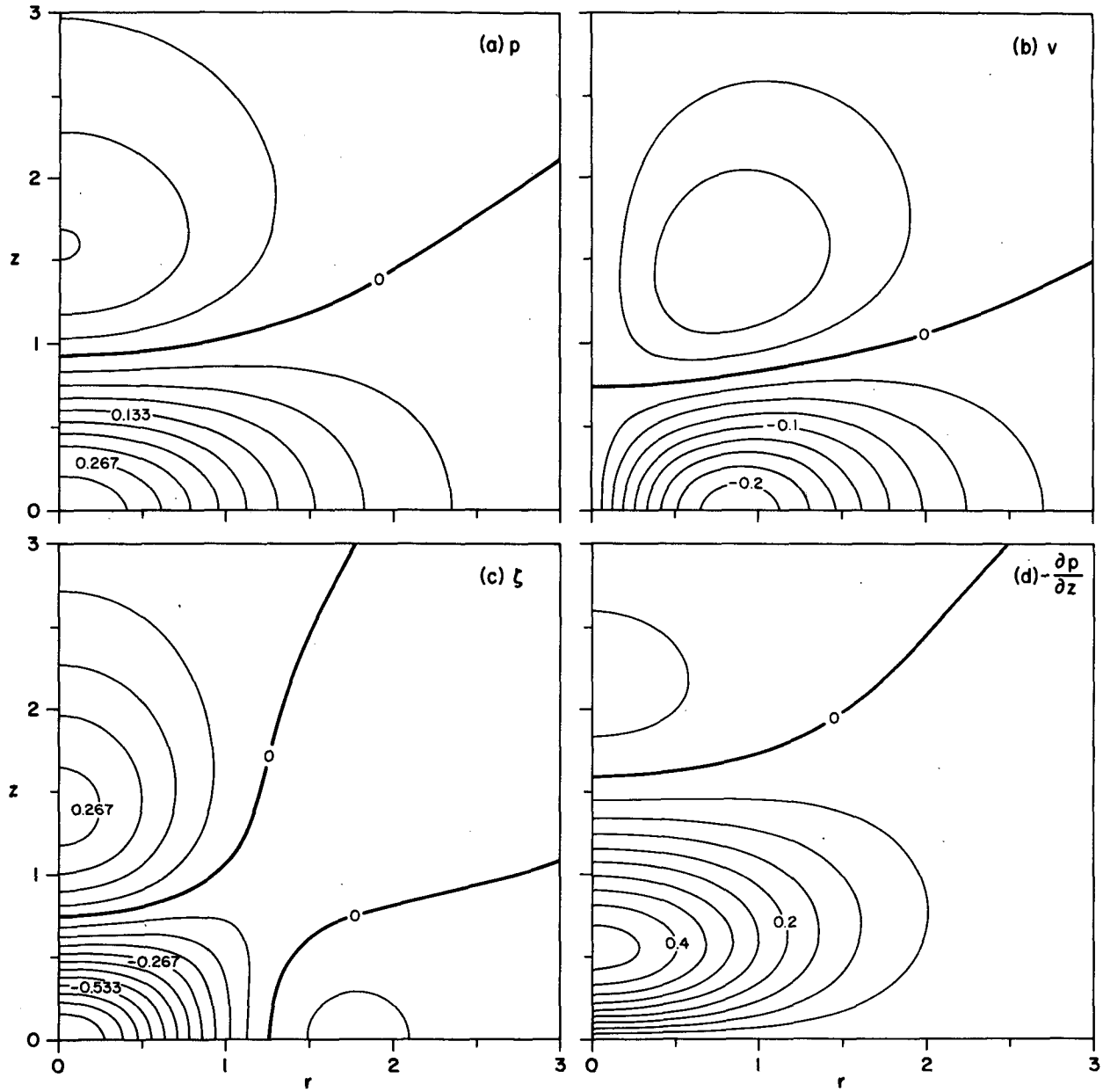

FIG. 3. For $\gamma = 0.25$, $\beta = 1$, $r_{0m} = 1$: (a) p_s, c.i. = 0.033; (b) v_s, c.i. = 0.025; (c) ζ_s, c.i. = 0.067; (d) $-\frac{\partial p_s}{\partial z}$, c.i. = 0.05; (e) $\frac{\partial^2 p_s}{\partial z^2}$, c.i. = 0.133; (f) ξ, c.i. = 0.033; (g) η, c.i. = 0.033.

The solution fields show patterns for all γ which are similar to those in Figs. 2 and 3. One notable change is that the amplitude of the normalized potential vorticity difference (e.g., Fig. 2c) increases approximately as γ^2.

Next we examine dependences upon r_{0m}, which spans $(0, \infty)$. (It is appropriate to compare these with $b^{-1/2}$ variations in the layered problem.) The variation of SCV parameters is listed in Table 2. As the radial scale of the mixing anomaly decreases, the adjusted SCV increases in both R_s and B_s, and the shape deformation during adjustment increases. Azimuthal velocity and transport both show a maximum at intermediate (but different) values of r_{0m}. Energy loss increases as r_{0m} decreases, such that $(\mathrm{KE}_s + \mathrm{PE}_s)/\mathrm{PE}_m$ is proportional to r_{0m} for small r_{0m}, and the relative amount of kinetic energy after adjustment also increases. All of these features occur in the layered adjustment solution as well, even the intermediate r_{0m} peak of v and Tr extrema in (12), (13), and (19). One qualitative difference is that $\mathrm{KE}_s/\mathrm{PE}_s$ exceeds the value of one as $r_{0m} \to 0$, which is prohibited in (21).

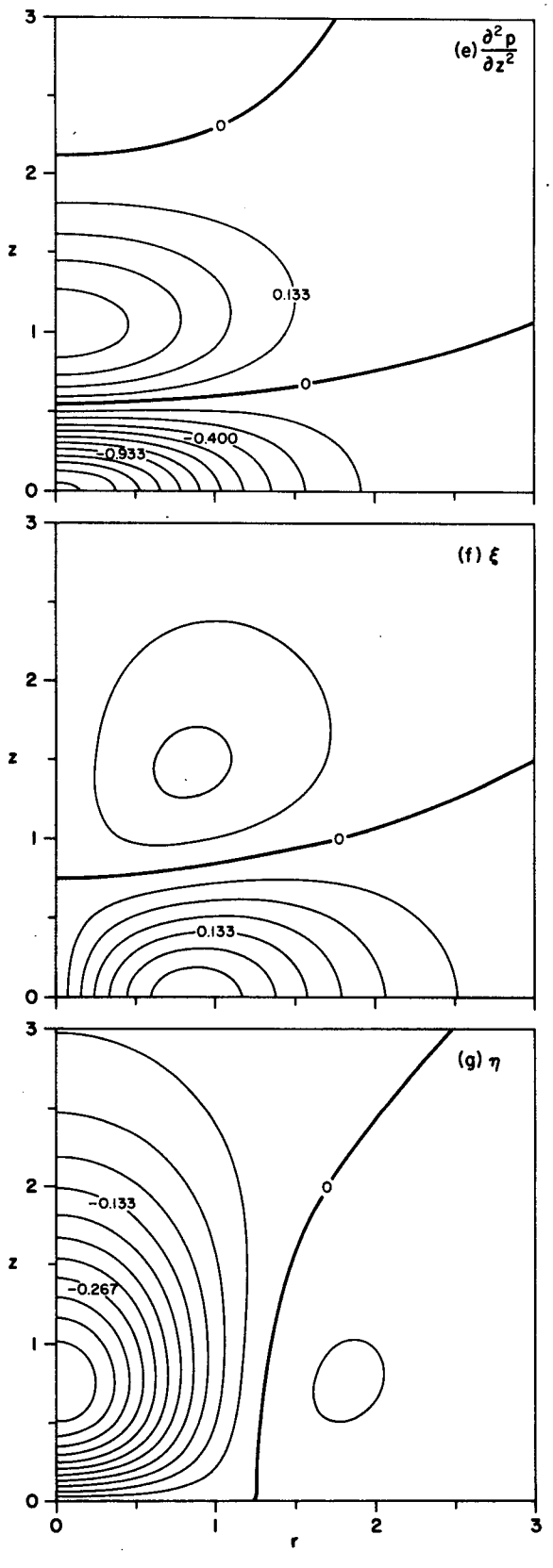

FIG. 3. (*Continued*)

The bounded amplitude measures of (50) are plotted in Fig. 5. The functional dependence on r_{0m} are strongly nonlinear. The asymptotic limits are

$$R_s \to \begin{cases} \left.\begin{aligned} &2\gamma(1-\gamma),\ \frac{R_s}{\gamma} \to 2(1-\gamma) \\ &B_s \to \infty,\ \frac{R_s}{2B_s} \to 0 \end{aligned}\right\} \text{ as } r_{0m} \to 0 \\ \left.\begin{aligned} &R_s \to 0,\ \frac{R_s}{\gamma} \to 0 \\ &B_s \to 0,\ \frac{R_s}{2B_s} \to 2\gamma \end{aligned}\right\} \text{ as } r_{0m} \to \infty \end{cases} \tag{54}$$

for $\gamma \neq 0$. The large r_{0m} limit is equivalent to no change in N^2 at the core during adjustment when the breadth of the mixed region becomes infinitely wide; the associated relative vorticity becomes vanishingly small. This limit is also found in the layered model as $b \to 0$. The small r_{0m} limit is equivalent to relative vorticity dominating vortex stretching at the core (i.e., $q_s(0, 0) \to Z(0, 0)$ as $r_{0m} \to 0$). Numerical verification of the small r_{0m} limit is limited by failure of iteration convergence in (43) at finite γ. The limitation is increasingly severe as $\gamma \to 1/2$; for example, at $\gamma = 0.25$ solutions could not be found for $r_{0m} < 0.04$, and at $\gamma = 0.4$ for $r_{0m} < 0.22$, and at $\gamma = 0.45$ for $r_{0m} < 0.26$. Nevertheless, for each of these γ values, the trends of R_s and B_s as $r_{0m} \to 0$ are consistent with (54).

Among the limits (53)–(54) there is only one apparent nonuniformity; viz.,

$$\lim_{r_{0m}\to 0} \lim_{\gamma \to 1/2} B_s = 0.25$$

$$\lim_{\gamma \to 1/2} \lim_{r_{0m}\to 0} B_s = \infty .$$

At finite, small r_{0m}, B_s is a strongly decreasing function of γ; for example, $B_s = 2.36$, 1.11 and 0.56 for $r_{0m} = 0.25$ and $\gamma = 0$, 0.25 and 0.40, respectively. Thus B_s can assume a wide range of values as the double limit in γ and r_{0m} is approached. In contrast, $R_s \to 1/2$ uniformly in γ and r_{0m}.

Variations with γ and r_{0m} are approximately superposable, in that the signs of ∂ (SCV parameters)$/\partial\gamma$ do not change with r_{0m}; the magnitudes, however, tend to increase as r_{0m} decreases.

Finally, we consider the influence of the shape of the mixing anomaly on the resulting SCV. In Table 3 are listed the SCV parameter dependences on β. What seems most remarkable is how small the parameter variations are. Those that are most sensitive are velocity and transport, which decrease as the radial pressure gradient diminishes with a smoother profile (smaller β), and the scale parameters z_{0s} and r_{0s}, which increase as β decreases and the far-field decay rate diminishes. Least sensitive are the relative energy loss and core stratification change [$R_s/2B_s$—see (48)] during ad-

TABLE 1. Amplitude dependence ($r_{0m} = \beta = 1$).

γ	R_s	B_s	z_{0s}	r_{0s}	$-v_{\min}$	$\mathrm{Tr}_{\max}$	$\frac{KE_s + PE_s}{PE_m}$	$\frac{KE_s}{PE_s}$
0	0	.334	.746	1.291	.205	0	.599	.402
.125	.095	.285	.705	1.320	.210	.006	.602	.395
.25	.181	.241	.663	1.350	.215	.012	.605	.389
.375	.257	.201	.619	1.382	.221	.018	.606	.385
.49	.316	.163	.574	1.420	.227	.023	.609	.379

justment. SCV parameter sensitivities are even less with smaller γ, particularly so in QG.

However, SCV shapes are sensitive to β. For large β, with a broad core region of relatively uniform N_m^2, the resulting SCV also has relatively uniform ζ, Z, N^2 and q in its core (Fig. 6).

5. A two-dimensional continuously stratified comparison

As with the layered solutions, we here present two-dimensional solutions to compare with the axisymmetric solutions of the previous section.

The nondimensionalization (32), parameter definitions (33), and mixing anomaly relations (34)–(35) apply to the 2D continuously stratified problem as well. The integrals PE, KE and $C(z)$ in (37), (38) and (52) are changed only by replacing $\int rdr$ with $\int dr$. Several relations in (36) and (38), however, do change since the 2D balance relation is exactly geostrophic:

$$A_m = r, \quad A_s = r + \frac{R}{r} v$$

$$v = \frac{\partial p}{\partial r}, \quad \zeta = \frac{\partial v}{\partial r}$$

$$Z = 1 + \frac{R}{4}\zeta, \quad q_s = Z \cdot N_s^2 - \frac{R\gamma}{4}\left(\frac{\partial^2 p}{\partial r \partial z}\right)^2. \quad (55)$$

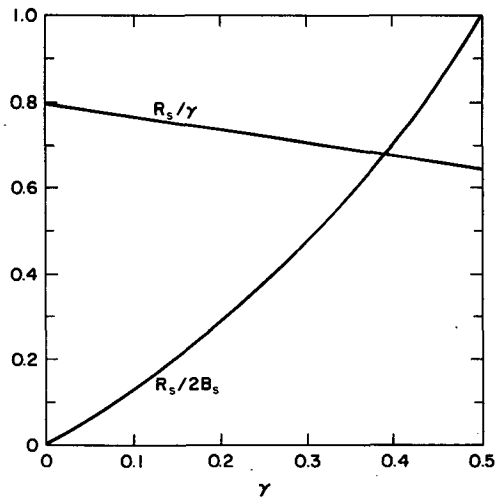

FIG. 4. Amplitude dependence of the SCV for $r_{0m} = \beta = 1$.

The 2D Lagrangian displacement relation is

$$\frac{\partial \xi}{\partial r} = -\frac{\partial \eta}{\partial z} + \gamma\left(\frac{\partial \xi}{\partial r}\frac{\partial \eta}{\partial z} - \frac{\partial \xi}{\partial z}\frac{\partial \eta}{\partial r}\right). \quad (56)$$

The adjustment problem is again as in (41)–(42), and an iterative solution method analogous to (43) is used. The SCV parameter definitions (48)–(49) are altered only to accommodate 2D geostrophic balance; viz.,

$$Z(0, 0) = 1 - \frac{1}{2} R_{s,2D}. \quad (57)$$

Hence the parameter bounds (50) become

$$R_{s,2D} \leq 2, \quad R_{s,2D} \leq 2B_{s,2D}. \quad (58)$$

A comparison of SCV parameters between 2D and axisymmetric adjustment is given in Table 4. In the axisymmetric geometry the SCV is stronger in vorticity [smaller $Z(0, 0)$]; it is weaker in velocity; it has undergone a greater decrease in height (smaller z_{0s}) and in aspect ratio (smaller B_s); its relative energy loss is greater; and its fraction of kinetic energy is greater. Each of the preceding statements was found to be true in the layered adjustment solutions (section 3). The one qualitative discrepancy is that r_{0s}/r_{0m} is somewhat smaller in the axisymmetric geometry for a continuously stratified fluid, whereas it usually is slightly larger in this geometry for a layered fluid [n., (13), (28) and (30)].

The 2D SCV variations with the parameter r_{0m}, β and γ are not qualitatively different from the the axisymmetric ones. However, the quantitative differences do increase as r_{0m} decreases. This is illustrated in Fig. 7. Note the larger extent and peak amplitudes of the SCV density anomaly and velocity in 2D. The amplitude peaks in 2D are also located further from the origin, so that the derivative quantities $\gamma^{-1}(N^2 - 1)$ and ζ are weakened near the core relative to the axisymmetric solutions. This competition between scale and amplitude is such that $-\zeta$ is larger in the axisymmetric solution, while $-\gamma^{-1}(N^2 - 1)$ is larger in 2D. (Conservation at the origin precludes both quantities being larger in either geometry.) Specifically, the core values for the solution in Fig. 7 with $r_{0m} = 0.25$, $\gamma = 0.4$, and $\beta = 1$ are the following.

axisymmetric:

$$Z(0, 0) = 0.332$$

$$N_m^2(0, 0) = 0.604$$

TABLE 2. Horizontal size dependence ($\gamma = 0.4$, $\beta = 1.0$).

r_{0m}	R_s	B_s	z_{0s}	$\frac{r_{0s}}{r_{0m}}$	$-v_{\min}$	$\mathrm{Tr}_{\max}$	$\frac{\mathrm{KE}_s + \mathrm{PE}_s}{\mathrm{PE}_m}$	$\frac{\mathrm{KE}_s}{\mathrm{PE}_s}$
2.0	.141	.092	.736	1.212	.191	.008	.808	0.168
1.0	.272	.193	.609	1.387	.222	.019	.606	0.386
0.5	.387	.334	.487	1.685	.207	.026	.372	0.763
0.25	.445	.561	.394	2.103	.156	.022	.185	1.343

2D:

$$Z(0, 0) = 0.531$$
$$N_m^2(0, 0) = 0.377. \tag{59}$$

Analogs to the limiting relations (53)–(54) also hold in 2D, modified only by the altered bounds (58):

$$R_s \to 0 \quad \text{as} \quad \gamma \to 0$$
$$\frac{R_s}{2B_s} \to 1 \quad \text{as} \quad \gamma \to \frac{1}{2}$$
$$R_s \to 4\gamma, \quad B_s \to \infty \quad \text{as} \quad r_{0m} \to 0$$
$$\frac{R_s}{2B_s} \to 2\gamma, \quad B_s \to 0 \quad \text{as} \quad r_{0m} \to \infty. \tag{60}$$

To approach closely the $r_{0m} = 0$ limiting values, though, requires much smaller values of r_{0m} in 2D than in the axisymmetric case; for example, the value of $Z(0, 0)$ is much farther from zero for 2D in (59) than it is in the axisymmetric case.

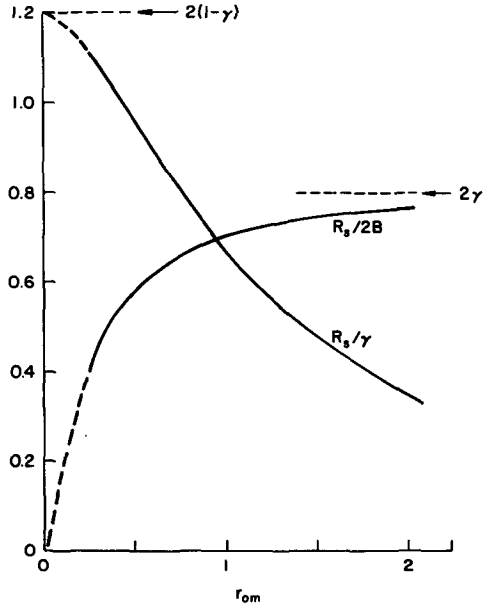

FIG. 5. Radial size dependence of the SCV for $\gamma = 0.4$ and $\beta = 1$. Arrows mark the asymptotic limits in (54), and the dashed lines are interpolations between calculated values and the $r_{0m} = 0$ limit.

6. Energy ratio

There has been considerable interest recently in the ratio of locally generated kinetic energy to potential energy locally released during geostrophic adjustment. This is defined by

$$e \equiv \frac{\mathrm{KE}_s}{\mathrm{PE}_m - \mathrm{PE}_s}. \tag{61}$$

Previous calculations of e have been based upon various vertically sparse representations (as in the layered calculations of sections 2 and 3). Van Heijst and Smeed (1986) remarked that the adjustment solutions of Rossby (1938), Gill (1976), and Van Heijst (1985) all have the value $e = \frac{1}{3}$, and they speculated that this might, in some sense, be a universal value. Ou (1986) remarked that a family of solutions with initially weak density gradients has the value $e = \frac{1}{2}$, and e decreases to $\frac{1}{3}$ as the initial gradients become arbitrarily steep. Middleton (1987) obtained solutions in which e is bounded from above by the value $\frac{1}{2}$ and is a monotonically decreasing function of the ratio of the deformation radius to the dominant horizontal scale of the initial anomaly; this ratio is equivalent to $b^{1/2}$ (which is proportional to r_{0m}^{-1}) in the layered representation and to r_{0m}^{-1} in the nondimensional continuously stratified representation. Van Heijst and Smeed (1986) demonstrated similar behavior (except with an upper bound of $\frac{1}{3}$) where distance to a nearby lateral boundary provides an additional horizontal scale.

The present solutions can also be examined for their e values. The layered solutions [(22) and (31)] have

axisymmetric:

$$e = \frac{T^{-1/2}(2 + T^{-1/2})}{(1 + T^{-1/2})(3 + T^{-1/2})}$$
$$\in \left[0, \frac{3}{8}\right]$$
$$\to \frac{1}{3\sqrt{2}} b^{-1/2} \propto r_{0m} \text{ as } b \to \infty \text{ or } r_{0m} \to 0$$

TABLE 3. Shape dependence ($\gamma = 0.4$, $r_{0m} = 1$).

β	R_s	B_s	$\frac{R_s}{2B_s}$	z_{0s}	r_{0s}	$-v_{\min}$	$\mathrm{Tr}_{\max}$	$\frac{\mathrm{KE}_s + \mathrm{PE}_s}{\mathrm{PE}_m}$	$\frac{\mathrm{KE}_s}{\mathrm{PE}_s}$
2.00	.257	.180	.713	.565	1.332	.282	.031	.616	.360
1.50	.264	.186	.709	.574	1.332	.256	.026	.613	.370
1.00	.272	.193	.705	.609	1.387	.222	.019	.606	.386
0.75	.278	.198	.700	.668	1.501	.203	.015	.604	.390

2D:

$$e = \frac{1}{2} U^{-1/3} \epsilon\left[0, \frac{1}{2}\right] \to \frac{1}{2 \cdot 2^{1/3}} b^{-1/3} \propto r_{0m}^{2/3} \text{ as } b \to \infty \text{ or } r_{0m} \to 0. \quad (62)$$

In both geometries e is bounded from above and decreases monotonically with r_{0m}^{-1}. Note, however, the differing upper bounds and the differing asymptotic power laws.

The continuously stratified solutions (sections 4 and 5) have the remarkable property that e is independent of the model amplitude and shape parameters, γ and β, for both axisymmetric and 2D geometries. Of course, the confidence with which this conclusion can be drawn is limited by the numerical accuracy of the solutions, which I believe to be better than 2% in e throughout the parameter ranges surveyed above. The particular value does depend on the geometry, however: for axisymmetric solutions with $r_{0m} = 1$, $e = 0.30(0)$, whereas for 2D $e = 0.33(3)$. The third significant digits should be viewed somewhat skeptically: if e truly is independent of γ and β, then I estimate the uncertainty in e to be no more than ± 0.002.

In the continuous solutions e also decreases monotonically with r_{0m}^{-1}. While neither of the limits for r_{0m} (i.e., 0 and ∞) has been examined to an extreme degree (because of numerical limitations), both the $r_{0m} \to \infty$ upper bounds and the $r_{0m} \to 0$ power laws for e in the layered solutions (62) seem to be approximately valid for the continuous ones as well, in both axisymmetric and 2D geometries.

In summary, the energy ratio e does exhibit a considerable degree of insensitivity to the initial anomaly profile shape and intensity, and it does vary within a relatively narrow range as a function of the normalized anomaly aspect ratio or as a consequence of the geometry. There seems to be no greater degree of universality for e than this.

7. Discussion

We have examined solutions of the fully nonlinear, finite Rossby number (i.e., balanced) adjustment problem in an axisymmetric geometry. The parameter dependences upon initial stratification strength (how well mixed the anomaly is), aspect ratio, and profile shape have been explored. Comparisons have been made with solutions in a coarse layered representation, in the quasi-geostrophic limit, and in a two dimensional geometry. All of these comparison situations exhibit qualitatively similar solutions, but in each case the quantitative differences are appreciable.

SCVs typically have been observed long after their generation. Their characteristic parameters do not appear to have universal values, nor do radial or vertical profiles appear to have universal forms, although these

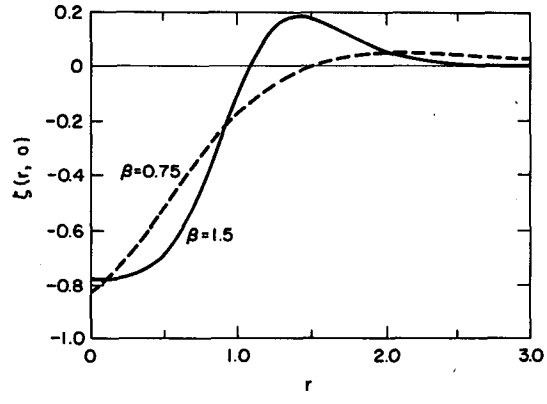

FIG. 6. Vorticity profiles for different β values ($r_{0m} = 1$, $\gamma = 0.4$).

TABLE 4. A two-dimensional comparison ($\gamma = 0.4$, $r_{0m} = 1$, $\beta = 1$).

	Axisymmetric	Two-dimensional
$\frac{R_s}{\gamma}$	0.680	0.929
$Z(0, 0)$	0.675	0.814
B_s	0.193	0.246
$\frac{R_s}{2B_s}$	0.705	0.754
z_{0s}	0.609	0.732
r_{0s}	1.387	1.475
$-v_{\min}$	0.222	0.274
$\frac{\mathrm{KE}_s + \mathrm{PE}_s}{\mathrm{PE}_m}$	0.606	0.759
$\frac{\mathrm{KE}_s}{\mathrm{PE}_s}$	0.386	0.187

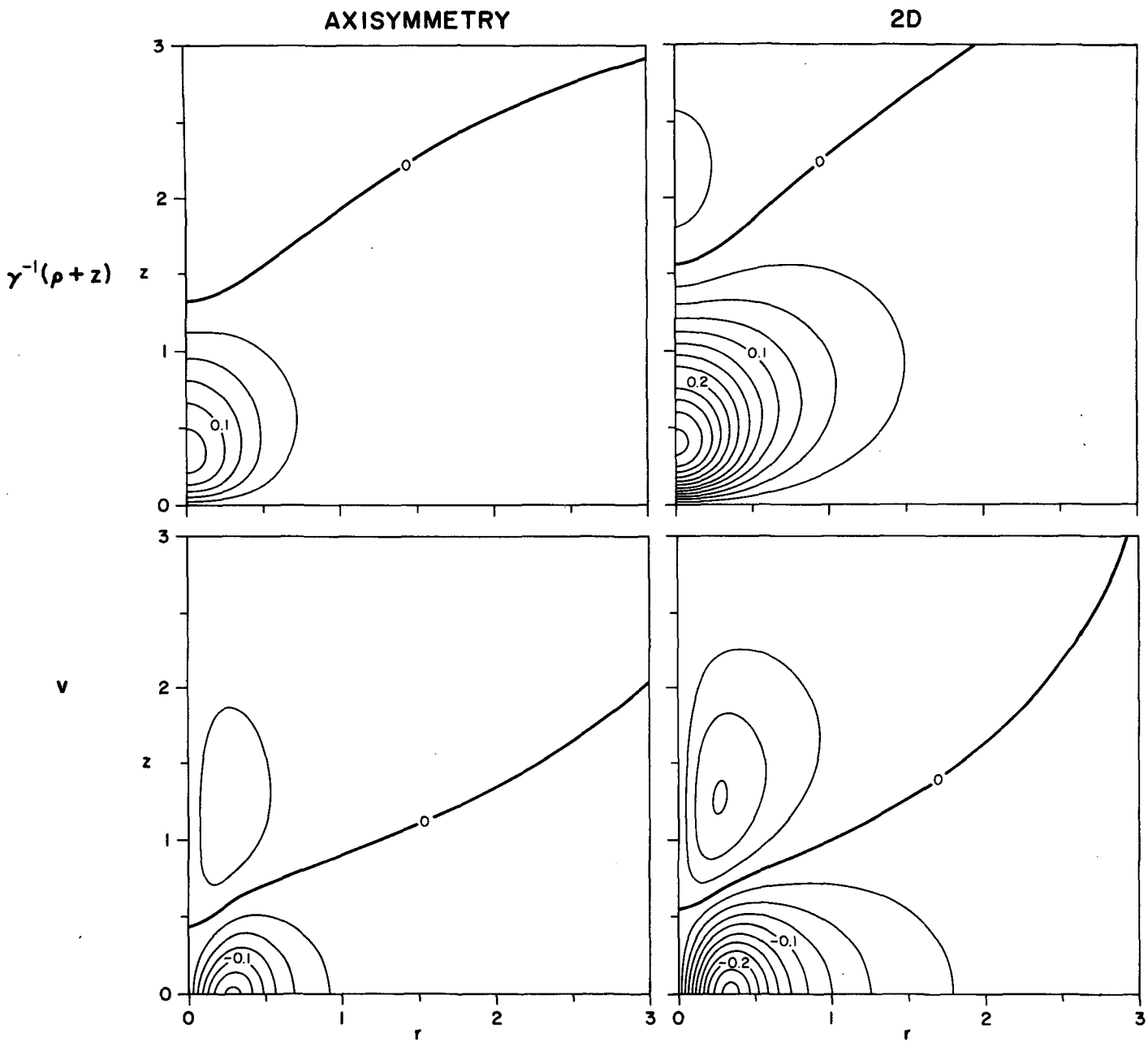

FIG. 7. SCV density anomaly and velocity fields for $\gamma = 0.4$, $r_{0m} = 0.25$, $\beta = 1$. Contour intervals are 0.025.

latter are difficult to measure (McWilliams 1985). It is possible that this lack of universality develops during the long lifetimes of SCVs from generation events which produce more universal forms, although I doubt it. In any event, we have seen here that variety in the initial states created by mixing yields variety in the SCVs. Suggestions of possible universality have been made by recent observers: Armi (personal communication) has observed a core region of approximately constant vorticity in a Mediterranean Outflow SCV, and D'Asaro (1988a) has observed cores of almost zero absolute vorticity in Bering Sea SCVs. We have seen that such states can occur through adjustment under certain circumstances. An extended core region of nearly constant vorticity results from a mixing anomaly of nearly constant N^2 (n., this occurs for large β values in our model profile). Zero absolute vorticity at the SCV core is approached as the aspect ratio of the mixed region becomes large (n., this is the small r_{0m} limit in our profile) and by near neutral stability in the core (large γ). Large aspect ratio (large compared to f/N, which is typically small) and near neutral stability are

not implausible for strong mixing events which arise from processes not importantly controlled by Coriolis effects, such as buoyant convection or shear flow instability.

The adjustment problems solved here are highly idealized ones, because of the assumptions of inviscid, adiabatic motion, axial and vertical symmetry, uniform stratification and rotation, and an infinite domain. However, I doubt that relaxation of these assumptions would make drastic changes in the resulting SCVs. Nonuniform stratification or vertical asymmetry will undoubtedly lead to vertical asymmetry in the SCV, but it likely will be interpretable mainly as a vertical coordinate stretching proportional to $N(z)$ (the Sargasso Sea SCV described by Elliot and Sanford 1986 has this property). Nonuniform Coriolis frequency should not matter much to mixing anomalies whose lateral dimensions are at most a few tens of kilometers. The present solutions also are valid with a solid, slippery boundary at $z = 0$, such as might result from stress-driven mixing at the sea surface or bottom. The solutions also apply to the situation of negative buoyancy forcing at the sea surface, leading to penetrative convection, entrainment, and sinking to an interior level of neutral buoyancy, as long as the final level is sufficiently deep; if the final level is only a little below the surface, the idealization of an infinite domain will be inapplicable. Mixing against lateral boundaries (as has recently been proposed for SCV generation by D'Asaro (1988b), although with finite velocity in the pre-adjustment state) also would have an important influence on the adjustment process, making it much more like 2D adjustment, unless the mixed patch is advected away from the boundary before adjustment occurs. Modest departures from axial symmetry also should not have a major influence, because the balancing circulation, as it develops during adjustment, will be efficient in symmetrizing the SCV through nonlinear interactions (Melander et al. 1987); this process, however, is not a wholly conservative one. Weak dissipation is unlikely to produce changes comparable to those occurring during adjustment, except on very much longer time scales.

Finally, I remark that the idea, due to C. G. Rossby, of solving adjustment problems by means of Lagrangian conservation relations relating initial and final states is a very powerful one. It would be quite difficult to solve the time-dependent problems directly, even by computational methods. The lack of the latter, though, leaves several fundamental questions open. For any new circumstance, there is no certainty a priori of the existence of a solution of the type sought (evidently we have escaped this pitfall here, as have previous investigators). Nor is there any certainty of uniqueness in the adjusted state (although I have seen no indication of multiple solutions here). Finally, even if a unique solution exists, there may not be any evolutionary pathway leading to it (although it seems to me plausible that there often, if not always, would be one).

Acknowledgments. The decision to solve this problem was strengthened by challenges issued by Eric D'Asaro. Peter Gent and Joseph Tribbia were patient and helpful critics during the period of its solution. Questions raised by referees led to the addition of section 6. Research costs were bourne by the National Science Foundation through the National Center for Atmospheric Research.

REFERENCES

Blumen, W., 1972: Geostrophic adjustment. *Rev. Geophys. Space Phys.*, **10,** 485–528.

Csanady, G., 1979: The birth and death of a warm core ring. *J. Geophys. Res.*, **84,** 777–780.

D'Asaro, E., 1988a: Observations of small eddies in the Beaufort Sea. *J. Geophys. Res.*, **93,** 6669–6684.

——, 1988b: Generation of submesoscale vortices: A new mechanism. *J. Geophys. Res.*, **93,** 6685–6693.

Elliot, B., and T. Sanford, 1986: The subthermocline lens D1. Part 1: Description of water properties and velocity profiles. *J. Phys. Oceanogr.*, **16,** 523–548.

Flierl, G., 1979: A simple model for the structure of warm and cold core rings. *J. Geophys. Res.*, **84,** 781–785.

Gill, A., 1976: Adjustment under gravity in a rotating channel. *J. Fluid Mech.*, **77,** 603–621.

Ikeda, M., 1982: A simple model of subsurface mesoscale eddies. *J. Geophys. Res.*, **87,** 7925–7931.

McWilliams, J., 1985: Sub-mesoscale coherent vortices in the oceans. *Rev. Geophys.*, **23,** 165–182.

Melander, M., J. McWilliams and N. Zabusky, 1987: Axisymmetrization and vorticity-gradient intensification of an isolated two-dimensional vortex through filamentation. *J. Fluid Mech.*, **178,** 137–159.

Middleton, J., 1987: Energetics of linear geostrophic adjustment. *J. Phys. Ocean.*, **17,** 735–740.

Monin, A., and A. M. Yaglom, 1971: *Statistical Fluid Mechanics, Vol. I,* The MIT Press, 769 pp.

Obukhov, A., 1949: On the question of geostrophic wind. *Izv. Akad. Nauk SSSR Ser. Geograf.-Geofiz.*, **13,** 281–306.

Ou, H., 1986: On the energy conversion during geostrophic adjustment. *J. Phys. Oceanogr.*, **16,** 2203–2204.

Rossby, C., 1937: On the mutual adjustment of pressure and velocity distributions in certain simple current systems, 1. *J. Mar. Res.*, **1,** 15–28.

——, 1938: On the mutual adjustment of pressure and velocity distributions in certain simple current systems, 2. *J. Mar. Res.*, **1,** 239–263.

Van Heijst, G., 1985: A geostrophic adjustment model of a tidal mixing front. *J. Phys. Oceanogr.*, **15,** 1182–1190.

——, and D. Smeed, 1986: On the energetics of adjustment problems in stratified rotating fluids. *Ocean Modelling,* **No. 68,** 1–3.